IEEE Access
Multidisciplinary ⋮ Rapid Review ⋮ Open Access Journal

Received 10 November 2023, accepted 23 January 2024, date of publication 2 February 2024, date of current version 8 February 2024.

Digital Object Identifier 10.1109/ACCESS.2024.3361665

RESEARCH ARTICLE

Circuit Model of Q(t) Data at High Temperature and Evaluation of Delay Parameters

RYOTA KITANI, SHINYA IWATA, (Member, IEEE), AND TOMOKA TSUYA
Osaka Research Institute of Industrial Science and Technology, Izumi, Osaka 594-1157, Japan

Corresponding author: Ryota Kitani (kitanir@tri-osaka.jp)

This work was supported in part by the Japan Society for the Promotion of Science KAKENHI under Grant number JP23H01405.

ABSTRACT The use of DC power equipment in the industry has significantly increased in recent years. Consequently, it has become imperative for insulation materials to withstand high DC electric fields. The current integration method, Q(t) measurement, is one of the most useful and effective methods for measuring the time dependency of charges. However, the mathematical and physical models of Q(t) measurement remain undeveloped because acquired data are not completely analyzed, particularly the effect of delay parameters on the charge saturation time of insulators. Therefore, this study analyzes the delay characteristics of Q(t) data at a high temperature by solving differential equations with some approximations. In addition, experiments are performed using polyimide sample sheets. Consequently, the parameters defining the charging dynamics across different stages are determined, and the proposed approach can effectively estimate circuit properties data. Moreover, the results indicate that actual experimental data can be reconstructed using adequate parameters. Therefore, the proposed analysis method can be used for further discussions regarding the analytical estimation of charge saturation time, marking a significant advancement in the industry.

INDEX TERMS Circuit analysis, environmental testing, insulator, Q(t) measurement.

I. INTRODUCTION

Electric power devices dealing with high DC voltages, high electric fields, and complex environments have increased in recent years. Therefore, the need to enhance the reliability and durability of electric power equipment has become imperative. Consequently, the demand for research on the diagnosis of electrical insulators has also increased.

Q(t) measurement is a diagnostic technique used for electrical insulators in power devices, cables, and other equipment [1], [2], [3], [4], [5], [6], [7], [8], [9], [10], [11], [12], [13], [14]. Q(t) measurement was first demonstrated in the 1970s by Takada et al. [1]. The circuit mechanism and structure are similar to those of a leakage current detector, which can detect extremely small electric currents that indicate the incompleteness and/or the defects of electrical insulation inside insulators. In contrast to partial discharge (PD) diagnosis [15], [16], which is primarily used for oscillating voltage, Q(t) measurement is applicable to DC voltage applications.

The associate editor coordinating the review of this manuscript and approving it for publication was Ting Yang.

Several studies have been reported on Q(t) measurement. Hanazawa et al. demonstrated the relationship between the temperature and leakage current around a power device [4], [5]. Wang et al. applied Q(t) measurement to detect water treeing [6]. Wang et al. [7], Fujii et al. [8], [9], and Iwata et al. [10] demonstrated that leakage current increases with electrical treeing. Kadowaki et al. [14] performed simultaneous measurements to obtain synced data of Q(t) measurement and used the pulsed electro-acoustic (PEA) method and an equivalent circuit model of a cross-linked polyethylene (XLPE) cable to express PEA data.

Our previous research [11] indicated the importance of a detailed analysis of Q(t) measurement data, particularly in high-temperature environments. However, these data exhibit temperature dependency, making the analysis challenging.

Previous research assumed the circuit model shown in Fig. 1(a). This is because previous studies primarily focused on verifying the difference between samples and/or the pretreatment conditions. The circuit model is effective for Q(t) measurement data containing linear parts (against time) and constant charging speed. However, a mathematical

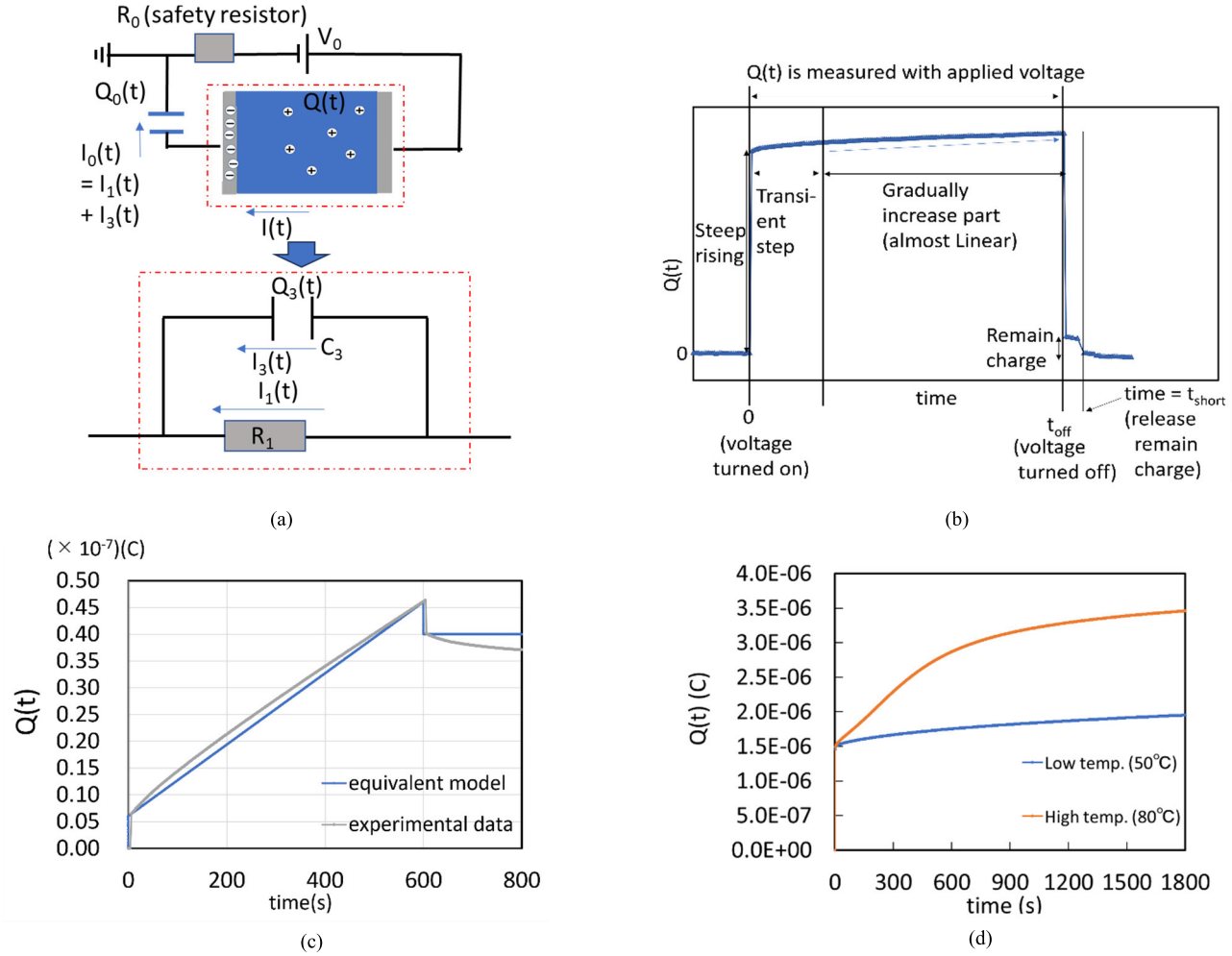

FIGURE 1. (a) Circuit model from a previous study, (b) typical experimental results, (c) difference between an experiment result at room temperature and the circuit model of (b), and (d) difference between the results at 50 °C and 80 °C.

model is required to analyze Q(t) measurement data in high-temperature environments and compare them with other experiment and simulation results, such as PEA data. Moreover, mathematical and physical models for distinguishing the transition from absorption to leakage current based on experimental results have not been developed, despite this being one of the advantages of using Q(t) measurement over other leakage current detection methods. This presents substantial risks in actual diagnoses owing to the lack of proper understanding and treatment of experimentally obtained Q(t) measurement values.

Therefore, this study focuses on the parameter fitting of the delay characteristics of Q(t) measurement. Fig. 1(b) illustrates a typical result pattern of Q(t) measurements at room temperature (less than 35 °C). A previous study [10] used the Q(t) circuit model shown in Fig. 1(a) to analyze such data; however, this model does not represent the delay properties. Fig. 1(c) shows a schematic representation of a comparison between typical experimental Q(t) measurement data at room temperature and the reconstructed data from the solution of the circuit model shown in Fig. 1 (a) (note that the position of the start time (t = 0) of the two plots shown in Fig. 1(c) are slightly shifted intentionally to visually distinguish the steep rising process of each plot). In addition, Fig. 1(d) compares typical experimental data of Q(t) measurements at 50 and 80 °C. Fig. 1(c) and (d) show that after the initial charging at t = 0 s, the results for low-temperature conditions rapidly transitioned to a linear phase; by contrast, the results for high-temperature conditions had an extremely long transition time. This indicates that Q(t) data obtained under high-temperature conditions require a more complicated fitting model compared with those under low-temperature conditions.

This study proposes a novel circuit model. First, a differential equation is formulated and solved based on a circuit model of Q(t) measurements to obtain the delay parameters of a parallel connection of one capacitor, one resistor, and one capacitor–resistor series combination. Second, an estimation method for the circuit property parameters is introduced based on approximations of the solutions. The mathematical analysis reveals a relationship between the charges within the Q(t) meter and those estimated inside the insulation material, a concept similar to space charges. In addition, numerical testing is performed to assess the appropriateness and basic

features of the proposed method. Third, a regression analysis on the experimental data obtained from Q(t) measurements of polyimide (PI) sheet samples at 80 °C is performed. The performance of the proposed estimation method is evaluated by calculating the root mean square error (RSME). Finally, the relationship between the physical meaning and a material model of Q(t) measurement and the limitations of the estimation method are determined.

II. METHODS

The methodology is summarized as follows: First, a circuit model is described. Second, the differential equation of the model is solved. Third, parameters are estimated using the proposed procedure. Fourth, numerical tests are performed to verify the estimation method. Finally, experimental Q(t) data of PI sheet samples at 80 °C (PI 80 °C data) are fitted, and the material properties (expressed as circuit properties) are estimated.

A. CIRCUIT MODEL AND ORDINARY DIFFERENTIAL EQUATION OF A MODEL WITH ONE CAPACITOR, ONE RESISTOR, AND A SERIES-CONNECTED CAPACITOR–RESISTOR

Fig. 2 shows the novel circuit model of the Q(t) measurement comprising one capacitor, one resistor, and one series capacitor–resistor combination (3-parallel model). C_0, C_2, and C_3 denote the capacitances of the integral condenser and the delay and main condenser elements of the material, respectively. V_0 denotes the DC voltage. R_1 denotes the main resistance of the material, and R_2 denotes the delay resistance ($R_1 \gg R_2$). Based on Kirchhoff's laws, the differential equation is expressed as follows:

$$\begin{cases} V_0 - I_2R_2 - \frac{Q_2(t)}{C_2} - \frac{Q_0(t)}{C_0} - I_0R_0 = 0, & (1) \\ I_1R_1 - \frac{Q_3(t)}{C_3} = 0, & (2) \\ I_2R_2 + \frac{Q_2(t)}{C_2} = I_1R_1, & (3) \\ I_1 + I_2 + I_3 = I_0, & (4) \end{cases}$$

where $Q_0(t)$, $Q_2(t)$, and $Q_3(t)$ represent the charges within C_0, C_2, and C_3. I_0, I_1, I_2, and I_3 denote the currents through C_0, R_1, R_2, and C_3, respectively.

A 3-parallel model is assumed to behave like an insulator with voids, and it also contains charge-delaying parameters that serve as "a damper in an oscillating system" for electrical charges. Though limitations exist in separating the parameters (e.g., insulators, the gap between electrodes, and the effect of surface roughness cannot be separated), the model was selected primarily owing to its outlook and simplicity in the mathematical analysis. Section III-C presents a detailed discussion of the model.

In a normal case, $Q_2(t)$ has three exponential functions:

$$A\frac{d^3Q_2(t)}{dt^3} + B\frac{d^2Q_2(t)}{dt^2} + C\frac{dQ_2(t)}{dt} + DQ_2(t) = 0, \quad (5)$$

where

$$A = C_0C_3R_0R_2,$$

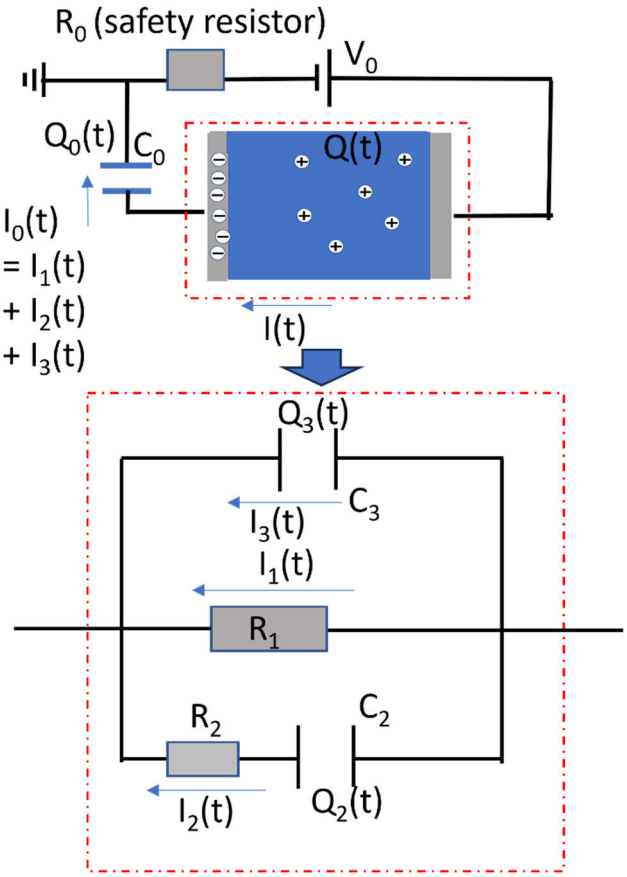

FIGURE 2. Circuit model containing the main resistance R_1 of the material, a series element comprising the capacitance C_2 and delay resistance R_2, the main capacitance C_3, and the integral condenser of the Q(t) meter.

$$B = \frac{C_0R_0R_2 + C_0R_0R_1}{R_1} + \frac{C_0C_3R_0 + C_0C_2R_2}{C_2} + C_3R_2,$$
$$C = \frac{(C_0R_1 + C_0R_0 + C_2R_2 + C_2R_1 + C_3R_1)}{C_2R_1},$$
$$D = \frac{1}{C_2R_1}.$$

A cubic formula (Cardano–Tartaglia formula) was used to solve the 3rd order differential equation. In general, the solutions of the cubic equation $AX^3+BX^2+CX+D = 0\,(\alpha, \beta, \gamma)$ are expressed as

$$\alpha = -\frac{B}{3A} - \sqrt[3]{\frac{3\sqrt{3}\,q + \sqrt{27q^2+4p^3}}{6\sqrt{3}}}\omega - \sqrt[3]{\frac{3\sqrt{3}\,q - \sqrt{27q^2+4p^3}}{6\sqrt{3}}}\omega^2, \quad (6)$$

$$\beta = -\frac{B}{3A} - \sqrt[3]{\frac{3\sqrt{3}\,q + \sqrt{27q^2+4p^3}}{6\sqrt{3}}}\omega^2 - \sqrt[3]{\frac{3\sqrt{3}q - \sqrt{27q^2+4p^3}}{6\sqrt{3}}}\omega, \quad (7)$$

$$\gamma = -\frac{B}{3A} - \sqrt[3]{\frac{3\sqrt{3}\,q + \sqrt{27q^2+4p^3}}{6\sqrt{3}}} - \sqrt[3]{\frac{3\sqrt{3}q - \sqrt{27q^2+4p^3}}{6\sqrt{3}}}, \quad (8)$$

where

$$p = \frac{-B^2 + 3AC}{3A^2}$$
$$q = \frac{2B^3 - 9ABC + 27A^2D}{27A^3},$$

and $1 + \omega + \omega^2 = 0$.

Subsequently, using the above solutions, the solution of the 3rd order differential equation in terms of $Q_2(t)$ is described as follows:

$$\therefore Q_2(t) = H_1 \exp(\alpha t) + H_2 \exp(\beta t) + H_3 \exp(\gamma t). \quad (9)$$

$Q_3(t)$ and $Q_0(t)$ also contain three exponential functions, expressed as follows:

$$Q_3(t) = \frac{C_3}{C_2}\{(C_2R_2\alpha + 1) H_1 \exp(\alpha t) + (C_2R_2\beta + 1)H_2 \exp(\beta t) + (C_2R_2\gamma + 1)H_3 \exp(\gamma t)\}, \quad (10)$$

$$Q_0(t) = \left(-M_1\alpha^2 - M_2\alpha - M_3\right) H_1 \exp(\alpha t) + (-M_1\beta^2 - M_2\beta - M_3)H_2\exp(\beta t) + (-M_1\gamma^2 - M_2\gamma - M_3)H_3 \exp(\gamma t) + C_0V_0, \quad (11)$$

where

$$M_1 = C_0C_3R_0R_2, \quad (12)$$
$$M_2 = \frac{(C_2R_1 + C_2R_2 + C_3R_1)C_0R_0}{C_2R_1} + C_0R_2, \quad (13)$$
$$M_3 = \frac{C_0R_0 + C_0R_1}{C_2R_1}. \quad (14)$$

Then, the following relationships are obtained by balancing the values of each circuit property: $M_1 \cong A, M_2 \cong B \cong C_0R_2$ and $M_3 \cong C \cong C_0/C_2$.

The boundary conditions are $Q_0(0) = Q_2(0) = Q_3(0)$. The analytic solution of H_1, H_2, and H_3 are expressed as follows:

$$H_1 = \frac{C_0V_0(\gamma - \beta)}{N_0}, \quad (15)$$
$$H_2 = \frac{C_0V_0(\alpha - \gamma)}{N_0}, \quad (16)$$
$$H_3 = \frac{C_0V_0(\beta - \alpha)}{N_0}, \quad (17)$$

where

$$N_0 = M_1\{\alpha^2(\gamma - \beta) + \beta^2(\alpha - \gamma) + \gamma^2(\beta - \alpha).$$

Note that $|\alpha| \ll |\beta| \ll |\gamma|$ and α, β, and γ are normally real negative values.

B. APPROXIMATION OF THE SOLUTION OF THE 3-PARALLEL MODEL PARAMETERS

Approximations are necessary to estimate the parameters of circuit properties from the solution(s) of the 3-parallel model. The approximations require some hypotheses. Note that for ease of explanation, a clear outlook is prioritized over mathematical rigidity in the subsequent sections.

Insulators typically exhibit extremely high resistances and low capacitances. By contrast, R_0 is generally on the 10 MΩ order at most, such that $R_0 \ll R_1$. In the case of $R_2 \ll R_1$, $C_3 \ll C_0$ and $C_2 \ll C_0$, the values of β, γ, H_1, H_2, and H_3 are approximated using Taylor expansion as follows:

$$\beta \cong -\frac{1}{C_2R_2}, \quad (18)$$
$$\gamma \cong -\frac{1}{C_3R_0}, \quad (19)$$
$$H_1 \cong C_2V_0, \quad (20)$$
$$H_2 \cong -C_2V_0, \quad (21)$$
$$H_3 \cong \frac{C_3R_0V_0}{R_2}. \quad (22)$$

Moreover, the rapid change in $Q_0(t)$ at the initial stage of charging (typically at $t < 1$ s) is approximated as C_3V_0. The nearly linear change in the latter part of charging (called the "linear part") is proportional to V_0/R_1, as shown in Fig. 3.

Details of the approximation process in this section are discussed in the preceding section of Appendix A.

C. ESTIMATION OF THE 3-PARALLEL MODEL PARAMETERS

Hereinafter, the $Q_0(t)$ stages are referred to as the "steep-change stage," "delay stage," and "linear stage," as shown in Fig. 3; these three stages correspond to γ, β, and α, respectively.

The estimation process is summarized as follows: Before the first step, R_0, V_0, and C_0 are considered to be known in advance because these values can be predetermined and/or measured in advance. First, as previously described in the last part of Section II-B, the gradient of the linear stage is nearly entirely dependent on the value of V_0/R_1, such that R_1 is easily obtained. Second, C_3V_0 is obtained through the steep-change stage, and its value is close to that of Q_3 (immediately after $t > 0$ s). Details of the approximation process in these steps are discussed in the latter section of Appendix A. Third, approximated $Q_2(t)$ data are obtained by subtracting C_3V_0 from $Q_0(t)$ in the early stage of the delay stage. Fourth, $Q_2(t)$ in the early stage of the delay stage is transformed and approximated as follows (using (20) and (21), with $\exp(\alpha t)$ and $\exp(\gamma t)$ nearly equal to 1 and 0 in the delay stage, respectively, because $|\alpha| \ll |\beta| \ll |\gamma|$):

$$Q_2(t) \cong H_1 + H_2 \exp(\beta t) \cong -H_2 + H_2 \exp(\beta t) \quad (23)$$

Subsequently, H_2 (and H_1) and β are obtained through regression using the approximated data of $Q_2(t)$ (e.g., exponential regression), such that C_2 and R_2 are estimated from (18)

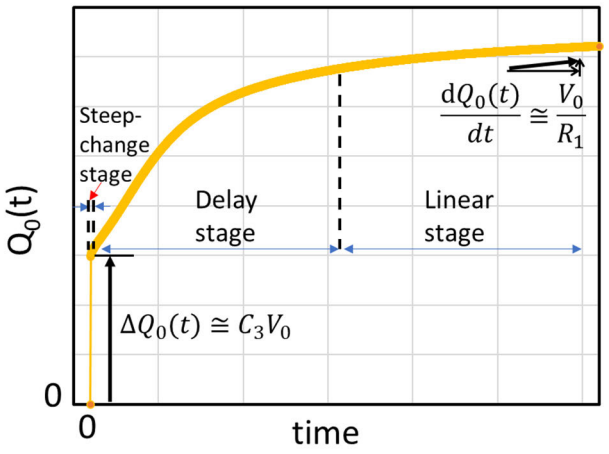

FIGURE 3. Representative image of the approximated values in the steep-change and linear stages.

and (20). Finally, α is obtained through an exponential function regression by substituting the circuit properties (C_0, C_2, C_3, R_0, R_1, R_2, and V_0) into (6). Note that β, γ, and other parameters except the circuit properties should be recalculated using the circuit properties and (7), (8), and (12)–(17) once all circuit properties are obtained because the high vulnerability of (11) cannot withstand even the slightest unsynchronized parameter change.

D. NUMERICAL TESTING

This section presents the numerical tests performed to evaluate the appropriateness of the estimation method presented in Section II-C. A "restoration test" was employed, which involved using imaginary data yielded by the predetermined values of the circuit constant. Two test conditions were considered referring to [10], as shown in Table 1. The timestep of creating the imaginary data was set to 1 s. This test assessed the difference between the original values of R_1, R_2, C_2, and C_3 and their estimated values. Furthermore, the estimated circuit properties were substituted into (9)–(11), and $Q_2(t)$, $Q_0(t)$, and $Q_3(t)$ were reconstructed. Finally, the difference between the estimated and original $Q_0(t)$ values was evaluated using the root mean squared error (RMSE).

E. REGRESSION OF EXPERIMENTAL RESULTS WITH THE 3-PARALLEL MODEL

A regression analysis on the experimental data obtained through the Q(t) measurement of PI was performed to apply the proposed method to an actual case. This regression estimates the actual cause of the delay parameters of an insulation material and specifies the detailed charging saturation time under the 3-parallel model. Owing to the hyperparameter used to decide the fitting range in the regression, the difference between the estimated and original $Q_0(t)$ values were evaluated using RSME after the regression, similar to the process described in Section II-D. Finally, the hyperparameter was determined using the calculated RSME to optimize the difference. Table 2 lists the experimental conditions and

TABLE 1. Input circuit properties and calculated true values of the parameters for different test conditions in numerical testing.

Parameter Name	Parameters of test cond. set (i) true val.	Parameters of test cond. set (ii) true val.
C_0	4.70E-07	4.70E-07
C_2	1.00E-10	2.00E-09
C_3	1.00E-09	1.00E-09
R_0	1.20E+07	1.20E+07
R_1	1.00E+13	2.00E+12
R_2	2.00E+10	4.00E+10
V_0	1000	1000
α	-2.123E-07	-1.057E-06
β	-0.4998	-0.0125
γ	-83.5609	-83.5361
H_1	9.98E-08	1.99E-06
H_2	-1.00E-07	-1.99E-06
H_3	6.00E-10	2.99E-10
M_1	1.13E+02	2.26E+02
M_2	9.46E+03	1.88E+04
M_3	4.70E+03	2.35E+02

circuit parameters, and Fig. 4 shows the experimental setup. A DC voltage supplier, a Q(t) measurement device (Q(t) meter) and an electrical insulator sample were connected serially. A heater was under the sample and the temperature condition was placed to 80°C. Samples were PI seats, and each seat was sized 100 × 100 mm. Humidity was not controlled, and the values moved from 36%RH to 57%RH. Note that the room temperature and humidity were checked at the start/end of each sample-measurement except the measurement of "003mQ" (the exception is due to the lack of data.) The upper electrode was a ϕ50 cylinder, and the lower electrode was a ϕ100 cylinder. The guard electrode (inner-ϕ60 cylinder) was set around the upper electrode. The electrodes were based on IEC 62631-3-1 and 3-2, which are standard for the measurement of volume/surface resistivity.

When t = 0, the DC voltage switch turned on and the set value was 1 kV. Charges started to accumulate at the Q(t) meter and the sample. Note that experimental data used in the regression are slightly modified because original experimental data contain data-missing and/or biases of zero position.

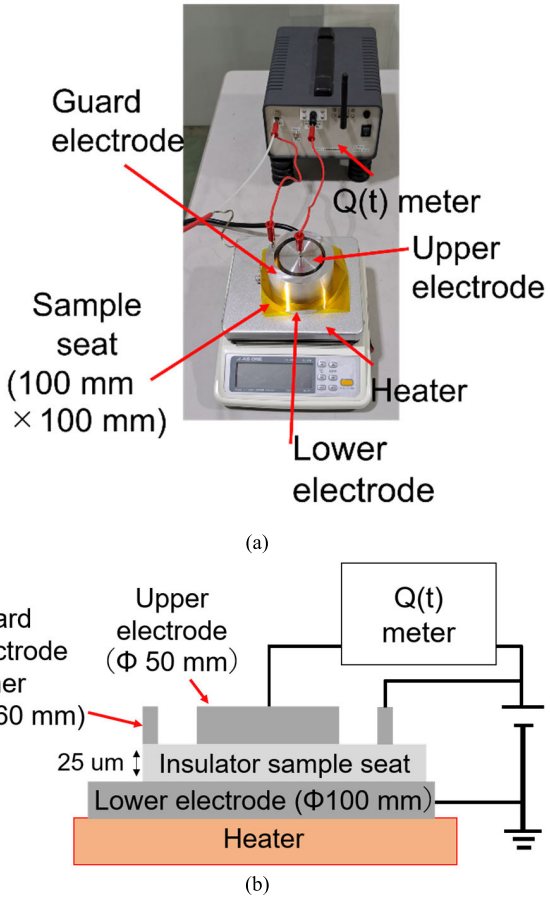

FIGURE 4. Experimental setup of Q(t) measurements of PI: (a) outline of the actual setup and (b) circuit outline.

TABLE 2. Experimental conditions and circuit parameters.

Thickness (μm)	Sample's temperature (°C)	Room temperature (°C)
25	80	21-26
Applied Voltage V_0 (kV)	C_0 (Capacitance of Integral Capacitor) (F)	Humidity (%RH)
1	4.7×10^{-6}	36-57

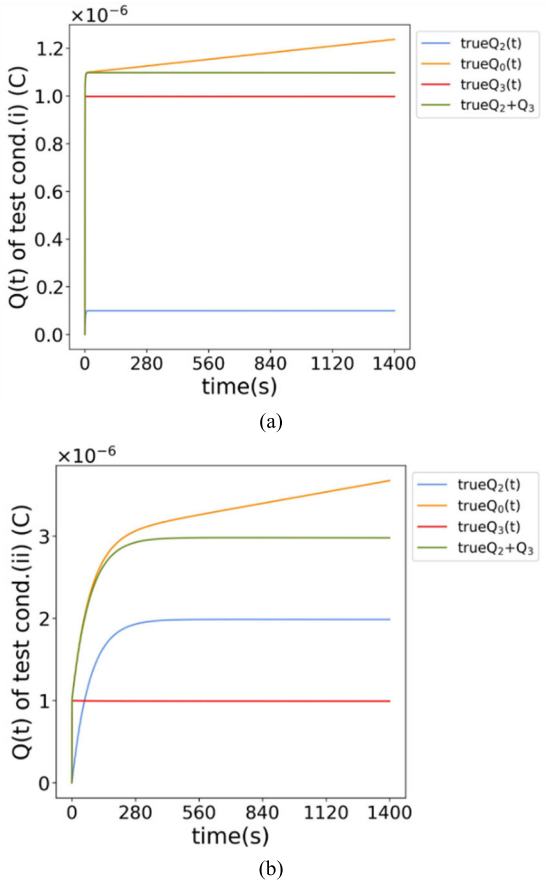

FIGURE 5. $Q_2(t)$, $Q_0(t)$, $Q_3(t)$, and $Q_2(t)+Q_3(t)$ numerically obtained by substituting the true values of C_2, C_3R_1, and R_2: (a) data obtained using the parameters of test condition set (i) and (b) data obtained using the parameters of test condition set (ii).

III. RESULTS AND DISCUSSIONS

A. RESULTS OF NUMERICAL TESTING ON THE 3-PARALLEL MODEL

Fig. 5(a) and (b) show the Q(t) data of $Q_0(t)$, $Q_2(t)$, $Q_3(t)$, and the summation of $Q_2(t)$ and $Q_3(t)$, created as imaginary data from the test condition sets (i) and (ii), respectively. Thus, these Q(t) data are theoretically correct values obtained using the parameters of the test condition sets.

Tables 3(a) and (b) list the estimated parameters from the numerical testing results of condition sets (i) and (ii), respectively. The fitting time range must be set as a hyperparameter; the fitting start time was set to 0 s, and the fitting end number row in Table 3 indicates the fitting end time. To optimize the fitting end time, values from 20 s to 140 s (in 10 s increments) were searched in test condition set (i) and from 150 s to 300 s (in 10 s increments) in test condition set (ii); the fitting end times selected based on the RMSE were 30 and 240 s, respectively. Table 3 also shows the ratio of the estimated circuit properties per the true. Fig. 6(a) and (b) show the plots of the estimated Q(t) data obtained by substituting all estimated circuit properties and the true $Q_0(t)$ data of test condition sets (i) and (ii), respectively.

Based on Table 3, the estimated circuit properties obtained from test condition set (ii) were consistent with the true values. By contrast, the estimated values obtained from test condition set (i) did not correspond with the true values. This was primarily because the time resolution of the steep-change stage was insufficient in test condition set (i); the time step was set to 1 s, but the first timestep (at approximately 0 s to 1 s) already encompassed the delay stage. A comparison between the estimated and true values of $Q_2(t)$ verified this. Consequently, the estimated value of $Q_2(t)$ after saturation in Fig. 6(a) ($= 6.37\times10^{-8}$C) was smaller than that of the true value in Fig. 5(a) ($= 9.97\times10^{-8}$C). In addition, the estimated and actual R_2 values differed. Therefore, a sufficiently small timestep results in more precise estimation values.

TABLE 3. Obtained circuit properties in numerical testing. (A) Result of test condition set (i) and (B) result of test condition set (ii).

	C_2(F)	C_3(F)	R_1(Ω)	R_2(Ω)
(true val.)	1.00E-10	1.00E-09	1.00E+13	2.00E+10
fitting end 20	6.291E-11	1.036E-09	1.00E+13	3.38E+10
fitting end 30	6.391E-11	1.036E-09	1.00E+13	3.50E+10
fitting end 40	6.491E-11	1.036E-09	1.00E+13	3.63E+10
(20/true)(%)	62.9%	103.6%	100.5%	169.0%
(30/true)(%)	63.9%	103.6%	100.5%	174.9%
(40/true)(%)	64.9%	103.6%	100.5%	181.3%

(a)

	C_2(F)	C_3(F)	R_1(Ω)	R_2(Ω)
(true val.)	2.00E-09	1.00E-09	2.00E+12	4.00E+10
fitting end 230	1.960E-09	1.023E-09	2.03E+12	3.71E+10
fitting end 240	1.978E-09	1.023E-09	2.03E+12	3.75E+10
fitting end 250	1.994E-09	1.023E-09	2.03E+12	3.78E+10
(230/true)(%)	98.0%	102.3%	101.4%	92.8%
(240/true)(%)	98.9%	102.3%	101.4%	93.6%
(250/true)(%)	99.7%	102.3%	101.4%	94.4%

(b)

TABLE 4. Obtained circuit properties through regression of experimental data of polyimid e at 80 °C.

sample name	fitting -end time	C_2 (F)	C_3 (F)	R_1 (Ω)	R_2 (Ω)
003mQ	1400	5.64E-10	1.43E-09	3.34E+13	7.68E+11
004mQ	1200	7.54E-10	1.46E-09	1.79E+13	4.95E+11
006mQ	1200	1.81E-09	1.48E-09	9.22E+12	2.37E+11
007mQ	900	4.00E-10	1.48E-09	1.81E+13	7.32E+11
010mQ	1300	1.12E-09	1.47E-09	1.73E+13	3.39E+11
011mQ	1300	1.48E-09	1.54E-09	1.28E+13	2.80E+11
012mQ	1200	5.10E-10	1.52E-09	1.63E+13	9.25E+11

Fig. 7(a) and (b) illustrate the effect of the timestep set to 1 and 0.1 s, respectively. These results indicate that the estimation method may fail to approximate $Q_3(t)$ if the timestep is extremely large, such that the time resolution is insufficient.

B. REGRESSION OF EXPERIMENTAL RESULTS

Fig. 8(a) shows the Q(t) measurement data of seven PI sheet samples at 80 °C. Fig. 8(b) shows an example of a polyimide sheet data at 50 °C for comparison purposed. In general, the graphs at 80 °C have much larger delay curves in the delay stage than those at 50 °C. Table 4 shows the estimated circuit properties obtained from regression of the experimental data. Similar to the numerical testing, the best fitting end time was selected based on the RSME. To optimize the fitting end time, values from 200 s to 2900 s (in 100 s increments) were searched for each sample.

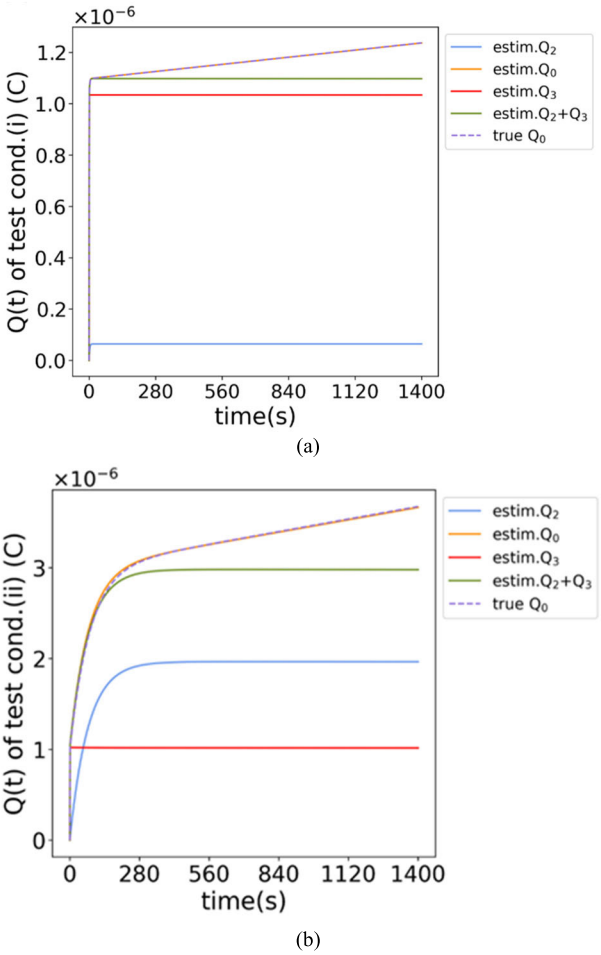

FIGURE 6. Reconstructed $Q_2(t)$, $Q_0(t)$, $Q_3(t)$, and $Q_2(t) + Q_3(t)$ numerically obtained by inputting the estimated values of C_2, C_3, R_1, and R_2 (solid lines) and the true value of $Q_0(t)$ shown in Fig. 5 (dotted lines): (a) data obtained using the parameters of test condition set (i) and (b) data obtained using the parameters of test condition set (ii).

Fig. 9 shows the plots of the estimated Q(t) data ($Q_0(t)$, $Q_2(t)$, $Q_3(t)$, and the summation of $Q_2(t)$ and $Q_3(t)$) of the PI sheet samples at 80 °C obtained by substituting all the estimated circuit properties. The figure also shows the plots of the true $Q_0(t)$ data. All plots indicated that the results of the estimated parameters (and their substitution to the approximated solution) successfully reconstructed the true experimental Q_0(t).

C. PRACTICAL AND PHYSICAL MEANING OF THE OBTAINED RESULTS AND CALCULATED PARAMETERS

α, β, γ, R_1, R_2, C_2, and C_3, parameters of Q(t) measurement in high-temperature conditions, were obtained in the previous sections, and α, β, and γ are time constants of the Q(t) data. Therefore, the following discussions focus on the remaining parameters: R_1, R_2, C_2, and C_3.

Fig. 10(a)–(c) show a series of explanations of how this study related the material and electromagnetic model to the circuit model. Fig. 10(a) shows an image of an insulator

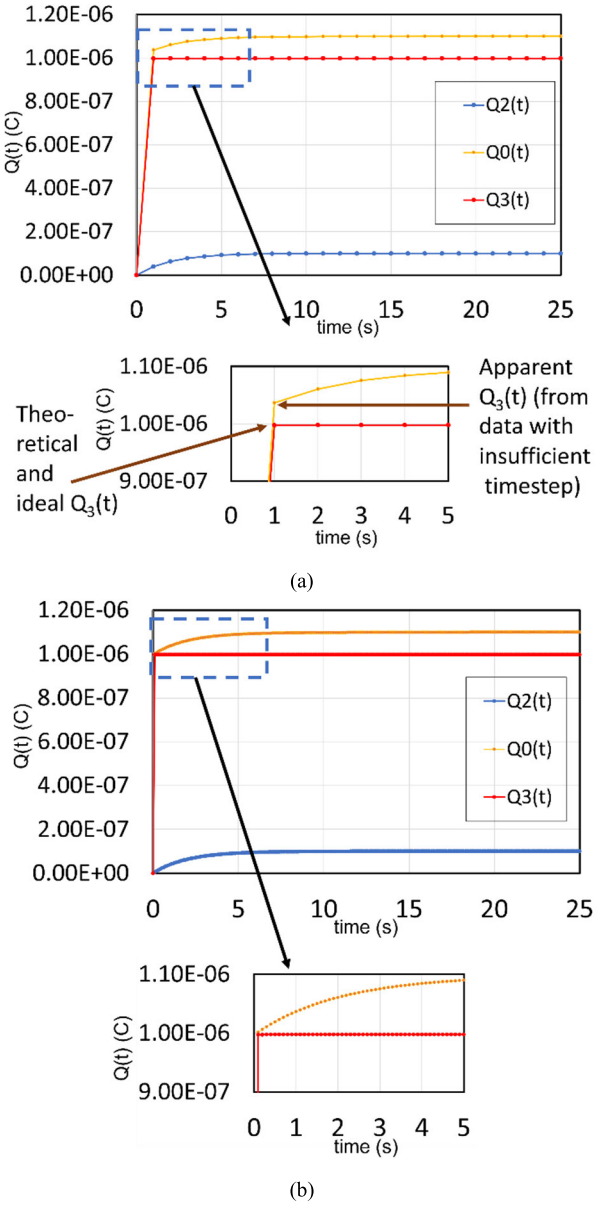

FIGURE 7. Illustrated risks of insufficient time resolution. (a) insufficient time step = 1 s and (b) sufficient time step = 0.1 s.

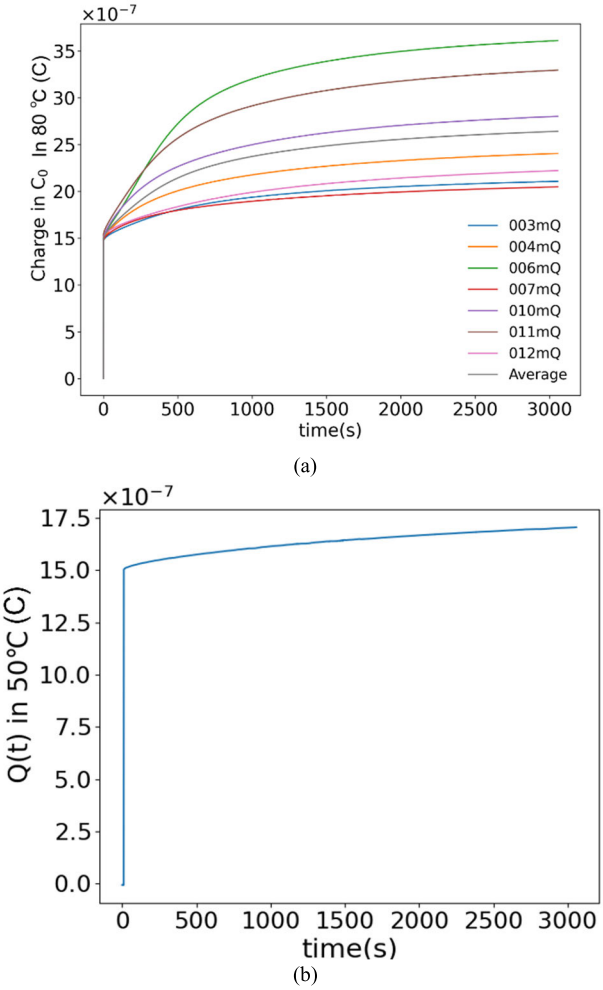

FIGURE 8. Q(t) data obtained through experiments at (a) 80 °C and (b) 50 °C.

with its internal charges under high-voltage conditions while obtaining Q(t) measurement data (the duration from the steep-change stage to the delay stage was considered). Subsequently, the charges between electrodes were assumed to move and be within the insulators. In the middle of Fig. 10(a), the distance between the leading edges of the positive and negative charges was assumed to be a time-dependent value, influencing the values of the R and C of the circuit as the charges move. Notably, in this model, this distance does not affect the basic structure of the circuit model of the material. In the bottom of Fig. 10(a), considering the material volume between the leading edges of the positive and negative charges, the structure of the material must be related to circuit properties.

As an example, a material model of an insulator or dielectric containing voids, defects, and/or impurities, was considered, such that the material is not a perfect (ideal) insulator. The volume can be considered as the composite of various parts of a conductor and perfect insulator. The structure of the insulator was approximated as a circuit model, as shown in Fig. 10(b). The approximation process is based on Fig. 10(a), the analogy of the homogenization method typically used for estimating macroscopic material properties (such as modulus) of composite materials [17], [18], and the basic circuit theory regarding the combination of multiple resistors or capacitors.

Disregarding the serial connection(s) of the models (for simplicity), the structure was simplified into a circuit element comprising a parallel combination of a capacitor, resistor, and series-connected capacitor and resistor. Accordingly, the proposed 3-parallel model is considered as one of the simplest models representing such structure, as shown in Fig. 10(c).

Considering the definitions of α, β, and γ, associating the 3-parallel model to the top of Fig. 10(a) reveals that C_3 corresponds to the main capacitor component indicating the accumulated charges on (and/or around) the subsurface

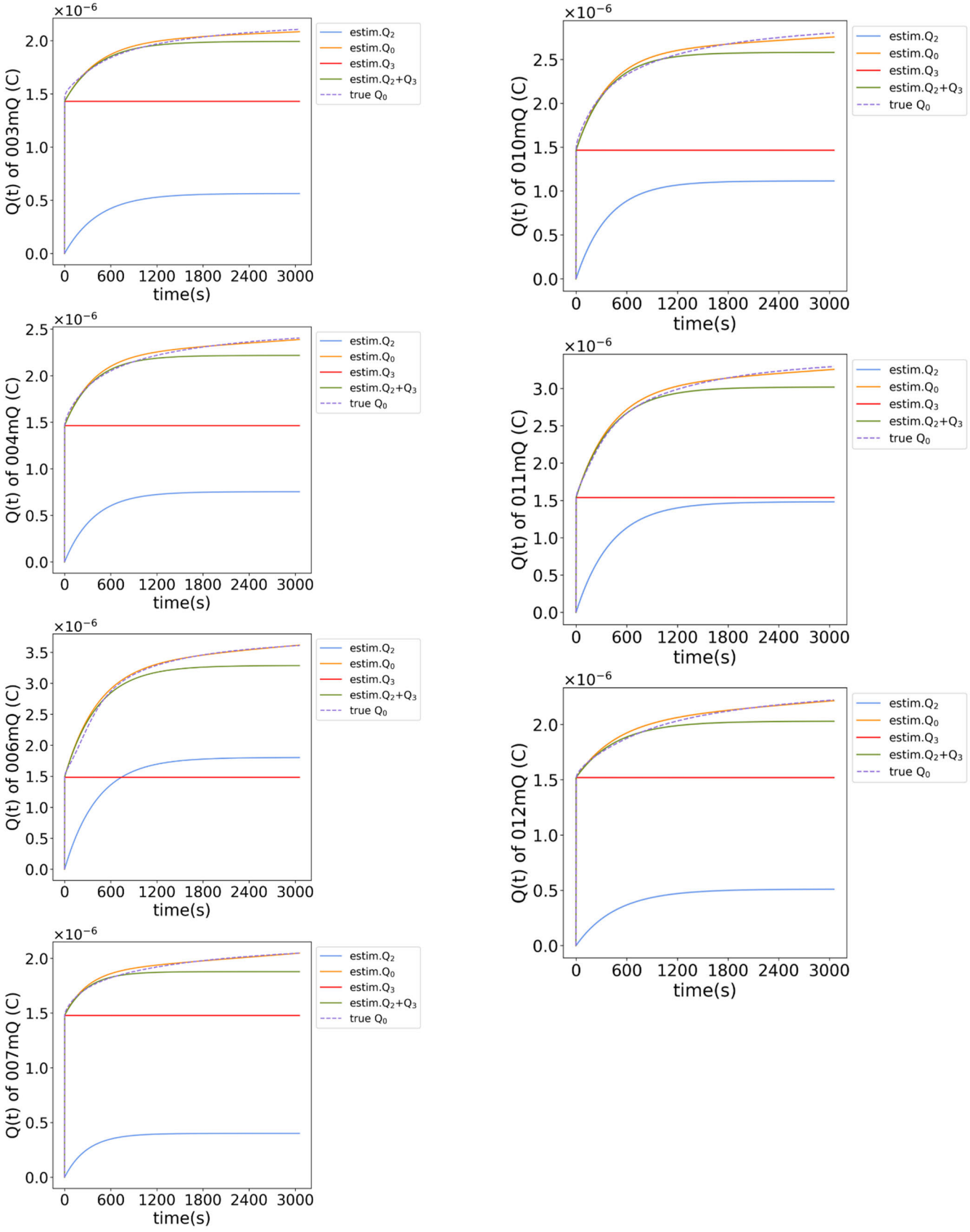

FIGURE 9. Reconstructed Q(t) data of PI at 80 °C based on the estimated values of the circuit properties. Each sample name corresponds to those in Fig. 8(a) and Table 4.

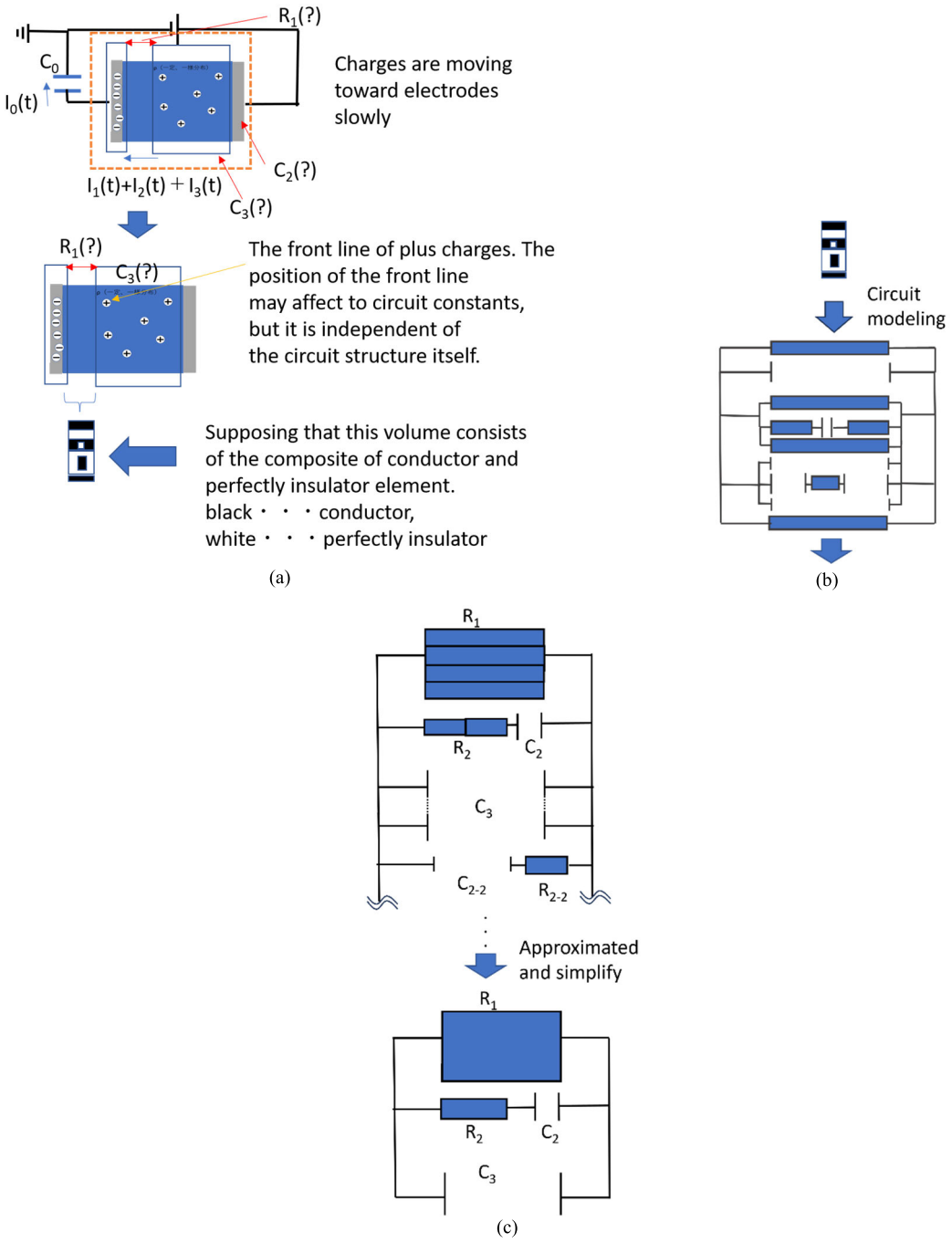

FIGURE 10. Explanation of the correlation between the material/electromagnetic model and circuit model: (a) image of an insulator with its intrinsic charges under high-voltage conditions and during Q(t) measurement, (b) circuit model considered from the analogy of estimating material properties of composite material, and (c) simplification of the circuit model resulting in the 3-parallel model.

between plate electrodes and an insulator. Similarly, C_2 corresponds to the capacitor subcomponent indicating the charges within the insulator between the plate electrodes, charging relatively slower than C_3. Furthermore, based on the discussion in Section II-B, R_1 functions as a conductor of pure leakage current, which is zero at the initial stage of Q(t) measurement, gradually increases in the delay stage, and become dominant in the linear stage. Similarly, R_2 serves as a conductor of the current comprising the charge transfer within the insulator, similar to the displacement current. Fig. 11 summarizes these details. Note that R_2 and C_2 are constant values that support the C_3 and R_1 configuration making the entire insulator equivalent to having a time-dependent resistor and capacitor.

Based on the above discussion, it can be inferred that $Q_2(t)$ is a concept similar to space charges within an insulator. Considering $Q_2(t)$ as indicative of the total amount of space charges, the proposed estimation method can also be con-

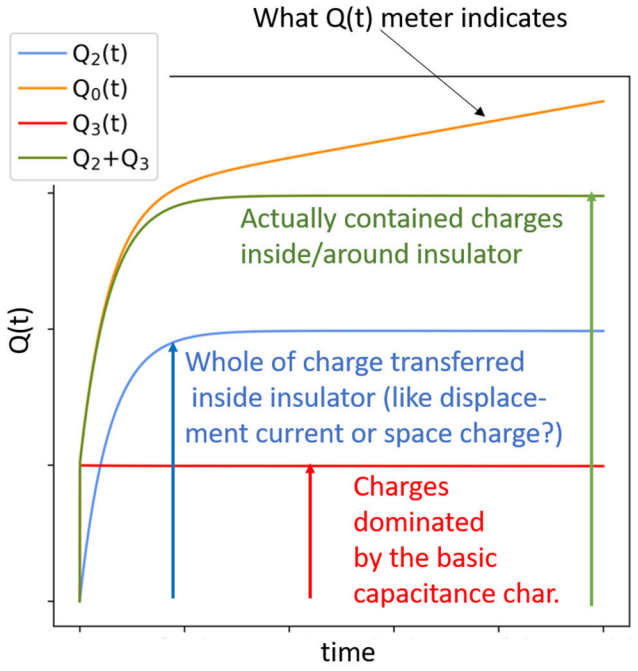

FIGURE 11. Details of the Q(t) data based on the 3-parallel model and its components.

sidered effective for estimating space charges from Q(t) data (hereinafter, the above hypothesis is referred to as the "$Q_2(t)$-hypothesis"). Moreover, the simulation can model the space charges that PEA may fails to measure owing to the limitation of the measurement setup.

Though the $Q_2(t)$-hypothesis is based on the assumption that the models mentioned in the earlier part of this section are accurate, the fitting results and the similarity between the estimated and experimental $Q_0(t)$ values indicate that the $Q_2(t)$-hypothesis cannot be fully rejected. Furthermore, as previously mentioned, the 3-parallel model is one of the simplest models that adequately represent the composite properties of the material and circuit model. Finally, the 3-parallel model is considered as a promising alternative for representing charge accumulation within an insulator.

D. LIMITATION OF THIS RESEARCH AND PROBLEMS ENCOUNTERED

As previously mentioned in Section III-A, when the target Q(t) data exhibit rapid changes in the steep-change stage that cannot be captured owing to the limited time resolution, the estimated circuit properties tend to deviate from the true values. The experimental limitation of the timestep should be improved to prevent this phenomenon. The experimental setup in this study had a 1 s timestep limitation. Under this constraint, the proposed method may not be applicable to samples at low temperatures. Otherwise, the calculations may yield values approximately twice or half of the true R_2/C_2 values.

From an optimization and fitting perspective, the best fitting end time obtained based on the RMSE may not necessarily yield the best circuit properties. For example, as shown in Table 3(a), the fitting end time that yielded the lowest RMSE was 30 s; however, the closest estimates to the true values of β and R_2 were obtained at 20 s, and the most accurate estimate for C_2 was obtained at 140 s. Therefore, the proposed estimation method strikes a balance among the parameters and may not provide the most accurate single-parameter estimates.

Two key limitations were identified in the modeling phase. First, the 3-parallel model can only accommodate simple time dependency of the R and C components of an insulator, and R_1, R_2, C_2, and C_3 are constant values. In addition, R_1 and R_2 are defined as resistors based on the Drude model [19], recognized as a standard model of metal conductivity. For more complicated time-dependent relationships, the ordinary differential equation should be changed considering the time dependency of the R and C components. Second, the 3-parallel model cannot account for the charge distribution within an insulator. Supplementary data using the PEA method (e.g., distribution shape or its ratio) is necessary for more detailed information regarding the charge distribution.

Therefore, extensive research on the theoretical and experimental methods is necessary to improve Q(t) measurements.

IV. CONCLUSION

The 3-parallel circuit model is significant for parameter fitting to analyze Q(t) data obtained under high-temperature conditions and achieve a deeper understanding of the physical meaning of the obtained data. In this research, a parallel circuit model comprising a capacitor, resistor, and series-connected capacitor and resistor was first developed as a representative insulator model under high-temperature conditions. Upon solving the 3rd order ordinary differential equations and approximating the solutions, an estimation method for the circuit properties was proposed based on the solutions. Subsequently, numerical testing of the proposed estimation method was performed. Finally, actual Q(t) data of a PI sheet samples at 80 °C were simulated, and the circuit properties were estimated. The following conclusions were drawn from the results:

1) Solving the differential equations determined the parameters that define the charging behavior in the steep-change, delay, and linear stages. These stages corresponded to the rapid increase in charges in the initial stage of Q(t) measurement, delay after initial charging, and nearly linear increments in the latter part of the measurement, respectively.

2) The numerical test results indicated that when the time resolution is sufficiently high (e.g., under a high-temperature condition), such that the borders of the steep-change and delay stages can be distinguished, the proposed estimation method could successfully obtain circuit properties data.

3) The regression of the experimental data revealed that the actual experimental data were consistent with the estimated values of the circuit properties and the 3-parallel model. Thus, the proposed estimation method can be used as a simple approximation method for analyzing charges within an insulator.

Based on the identified modeling and numerical analysis limitations, the following are suggested for future works:

1) When applying the proposed method for in-depth analysis of space charges in both time and spatial domains, the estimation method should incorporate more complex techniques, such as the combination of the PEA results and/or introduction of directly time-dependent resistor and/or capacitor components in the circuit model.

2) This research demonstrated the effects of applying a circuit model to a fundamental analysis of insulators. To address the effects that can be expressed only by quantum mechanics, the results obtained using the quantum mechanics/molecular dynamics (QM/MD) method should be considered.

APPENDIX A
APPROXIMATION OF PARAMETERS

A. APPROXIMATION OF PARAMETERS USED IN Q_2 (t)

A series of approximations was performed to express β, γ, H_1, H_2, and H_3 into simple forms using circuit properties C_0, C_2, C_3, R_0, R_1, and R_2, as described below.

When $\alpha, \beta,$ andγ are real values, the second and third terms of the right-hand side of (8) are almost equal to $-B/3A$ according to the Taylor expansion. Subsequently, γ is approximated, considering that the value of B is primarily influenced by C_0R_2. This approximation is expressed as follows:

$$\begin{aligned}\gamma &\cong -\frac{B}{3A} - 2\sqrt[3]{\frac{q}{2}} \\ &= -\frac{B}{3A} - 2\left\{\frac{B^3}{27A^3}\left(1+\frac{27A^3}{B^3}\cdot\frac{(3AD-BC)}{6A^2}\right)\right\}^{\frac{1}{3}} \\ &\cong -\frac{B}{A} \cong -\frac{C_0R_2}{C_0C_3R_0R_2} = -\frac{1}{C_3R_0}. \end{aligned} \tag{24}$$

In addition, based on (17) and (24), when $|\alpha| \ll |\beta| \ll |\gamma|$, H_3 is approximated as

$$H_3 = \frac{C_0V_0\,(\beta-\alpha)}{N_0} \cong \frac{C_0V_0}{M_1\gamma^2} = \frac{V_0}{C_3R_0R_2\gamma^2} \cong \frac{C_3V_0R_0}{R_2}. \tag{25}$$

Imaginary values based on ω should not be calculated to introduce the approximate form of β. Subsequently, under the premise that α and β are real minus values and considering the relationship of $|\alpha| \ll |\beta|$, β can be considered to be approximately equal to $\alpha+\beta$.

$$\begin{aligned}\beta \cong \alpha+\beta &= -\frac{2B}{3A} - \sqrt[3]{\frac{3\sqrt{3}\,q+\sqrt{27q^2+4p^3}}{6\sqrt{3}}}\left(\omega^2+\omega\right) \\ &\quad - \sqrt[3]{\frac{3\sqrt{3}\,q-\sqrt{27q^2+4p^3}}{6\sqrt{3}}}\left(\omega^2+\omega\right) \\ \therefore \beta &\cong -\frac{2B}{3A} + \sqrt[3]{\frac{3\sqrt{3}\,q+\sqrt{27q^2+4p^3}}{6\sqrt{3}}} \\ &\quad + \sqrt[3]{\frac{3\sqrt{3}\,q-\sqrt{27q^2+4p^3}}{6\sqrt{3}}} \end{aligned}$$

$$\left(\because \left(\omega^2+\omega+1=0\right)\right) \tag{26}$$

Since β should be a real value, and only $\sqrt{27q^2+4p^3}$ can produce the imaginary part in (26), $\sqrt{27q^2+4p^3}$ should be an imaginary value. In typical conditions involving circuit properties such as those discussed in this study, $|3\sqrt{3}\,q| \gg \sqrt{27q^2+4p^3}|$ is satisfied such that (27) is introduced using the Taylor expansion.

$$\begin{aligned}\beta &\cong -\frac{2B}{3A} + 2\sqrt[3]{\frac{q}{2}} \\ &= -\frac{2B}{3A} + 2\left\{\frac{B^3}{27A^3}\left(1+\frac{27A^3}{B^3}\cdot\frac{(3AD-BC)}{6A^2}\right)\right\}^{\frac{1}{3}} \\ &\cong -\frac{2B}{3A} + \frac{2B}{3A}\left\{1+\frac{1}{3}\cdot\frac{27A^3}{B^3}\cdot\frac{(3AD-BC)}{6A^2}\right\} \\ &\cong -\frac{2B}{3A}\cdot\frac{1}{3}\cdot\frac{27A^3}{B^3}\cdot\frac{BC}{6A^2} = -\frac{C}{B} \cong \frac{1}{C_2R_2} \end{aligned} \tag{27}$$

H_1 and H_2 can be introduced in a similar way as H_3 using (24) and (27):

$$H_1 = \frac{C_0V_0\,(\gamma-\beta)}{N_0} \cong \frac{C_0V_0}{M_1\gamma\beta} = \frac{V_0}{C_3R_0R_2\gamma\beta} \cong C_2V_0 \quad (= -\mathrm{H}_2)\,. \tag{28}$$

B. APPROXIMATION OF BASIC BEHAVIOR OF Q_0 (T)

Considering the approximation of $\mathrm{d}Q_0(t)/\mathrm{d}t$ in the linear stage, the gradient of $Q_0(t)$ at the stage can be introduced. When t is sufficiently high, $\exp(\beta t)$ and $\exp(\gamma t)$ are approximately equal to zero, such that

$$Q_0\,(t) \cong \left(-M_1\alpha^2 - M_2\alpha - M_3\right)H_1\exp(\alpha t) + C_0V_0, \tag{29}$$

and

$$\frac{\mathrm{d}Q_0\,(t)}{\mathrm{d}t} \cong \left(-M_1\alpha^3 - M_2\alpha^2 - M_3\alpha\right)H_1\exp(\alpha t)\,. \tag{30}$$

As previously discussed in Section II-A, $M_1 \cong A, M_2 \cong B, M_3 \cong C$. Accordingly, the right-hand side of (30) is approximated as follows:

$$\begin{aligned}&\left(-M_1\alpha^3 - M_2\alpha^2 - M_3\alpha\right)H_1\exp(\alpha t) \\ &\quad \cong -A\frac{\mathrm{d}^3Q_2\,(t)}{\mathrm{d}t^3} - B\frac{\mathrm{d}^2Q_2\,(t)}{\mathrm{d}t^2} - C\frac{\mathrm{d}Q_2\,(t)}{\mathrm{d}t} \\ &\quad = DQ_2\,(t) = \frac{H_1\exp(\alpha t)}{C_2R_1}. \end{aligned} \tag{31}$$

Using Taylor expansion,

$$\frac{H_1\exp(\alpha t)}{C_2R_1} \cong \frac{H_1}{C_2R_1}(1+\alpha t) \cong \frac{H_1}{C_2R_1} = \frac{V_0}{R_1}. \tag{32}$$

The rapid increase in $Q_0(t)$ in the steep-change stage is dominated by the coefficient of the $\exp(\gamma t)$ term. Using the relationships $M_1 \cong A, M_2 \cong B, M_3 \cong C$, the value of this rapid increase is expressed as follows:

$$-\left(-M_1\gamma^2 - M_2\gamma - M_3\right)H_3 \cong \frac{C_0R_2}{R_0C_3}H_3 = C_3V_0. \tag{33}$$

Notably, this value corresponds to the value of the rapid increase in $Q_3(t)$ attributed to the last term of the right-hand side of (10), such that the rapid increase in $Q_0(t)$ can be treated as approximately equal to $Q_3(t)$, as shown below:

$$-\frac{C_3}{C_2}\left(C_2R_2\gamma+1\right)H_3 \cong -C_3R_2\gamma H_3 = C_3V_0. \tag{34}$$

ACKNOWLEDGMENT

The authors would like to thank Tatsuo Takada, who is an emeritus professor with Tokyo City University, Hiroaki Uehara, who is a professor with Kanto Gakuin University, Tatsuki Okamoto, who is a visiting research scholar with Kanto Gakuin University, and Hiroshi Deguchi, who is a technical staff with the Osaka Research Institute of Industrial Science and Technology.

REFERENCES

[1] T. Takada, T. Saki, and Y. Toriyama, "Evaluation of electric charge distribution in polymer films," *Electr. Eng. Jpn.*, vol. 92, no. 6, pp. 28–35, Jan. 1972, doi: 10.1002/eej.4390920605.

[2] T. Takada, T. Fujitomi, T. Mori, T. Iwata, T. Ono, H. Miyake, and Y. Tanaka, "New diagnostic method of electrical insulation properties based on current integration," *IEEE Trans. Dielectr. Electr. Insul.*, vol. 24, no. 4, pp. 2549–2558, 2017, doi: 10.1109/TDEI.2017.006355.

[3] M. Fukuma and Y. Sekiguchi, "Current distribution measurement in insulating polymer cross section by current integration meter," in *Proc. Int. Symp. Electr. Insulating Mater. (ISEIM)*, Sep. 2017, pp. 73–76, doi: 10.23919/ISEIM.2017.8088692.

[4] D. Hanazawa, M. Mima, K. Hijikata, H. Miyake, Y. Tanaka, and T. Takada, "Evaluation of electric charge accumulation in insulation layer of power module using direct current integrated charge measurement," in *Proc. IEEE Int. Workshop Integr. Power Packag. (IWIPP)*, Toulouse, France, Apr. 2019, pp. 24–29, doi: 10.1109/IWIPP.2019.8799087.

[5] D. Hanazawa, K. Sonoda, H. Miyake, Y. Tanaka, and T. Takada, "Development of measurement system for DC integrated charge at high temperature," in *Proc. Condition Monitor. Diagnosis (CMD)*, Perth, WA, Australia, Sep. 2018, pp. 1–5, doi: 10.1109/CMD.2018.8535946.

[6] W. Wang, K. Sonoda, S. Yoshida, T. Takada, Y. Tanaka, and T. Kurihara, "Current integrated technique for insulation diagnosis of water-tree degraded cable," *IEEE Trans. Dielectr. Electr. Insul.*, vol. 25, no. 1, pp. 94–101, Feb. 2018, doi: 10.1109/TDEI.2018.006738.

[7] H. Wang, Z. Li, S. Zhou, M. Fan, Y. Wu, B. Du, and Z. Yang, "Relationship between electrical treeing degradation and DCIC-Q(t) characteristics of XLPE insulation," in *Proc. IEEE 4th Int. Conf. Dielectr. (ICD)*, Palermo, Italy, Jul. 2022, pp. 589–592, doi: 10.1109/ICD53806.2022.9863575.

[8] M. Fujii, M. Fukuma, S. Mitsumoto i, and Y. Sekiguchi, "Deterioration diagnosis of epoxy resin evaluated by current integration meter," in *Proc. Int. Symp. Electr. Insulating Mater. (ISEIM)*, Toyohashi, Japan, Sep. 2017, pp. 319–322, doi: 10.23919/ISEIM.2017.8088751.

[9] M. Fuiji, K. Matsushita, M. Fukuma, and S. Mitsumoto, "Study on characteristics of electrical tree in epoxy resin measured by current integrated charge method," in *Proc. Int. Symp. Electr. Insulating Mater. (ISEIM)*, Tokyo, Japan, Sep. 2020, pp. 177–180.

[10] S. Iwata, R. Kitani, and T. Takada, "Diagnostic technique for electrical tree by current integration method," in *Proc. IEEE Electr. Insul. Conf. (EIC)*, Calgary, AB, Canada, Jun. 2019, pp. 317–320, doi: 10.1109/EIC43217.2019.9046562.

[11] R. Kitani and S. Iwata, "Q(t)-measurements of electrically deteriorated polymeric materials under environmental testing," in *Proc. Int. Symp. Electr. Insulating Mater. (ISEIM)*, Tokyo, Japan, Sep. 2020, pp. 169–172.

[12] Y. Sekiguchi and M. Fukuma, "Electrical charges and currents distribution analysis in plaque samples by the DCIC-Q(t) method," in *Proc. Int. Symp. Electr. Insulating Mater. (ISEIM)*, Toyohashi, Japan, Sep. 2017, pp. 609–612, doi: 10.23919/ISEIM.2017.8166563.

[13] H. Ren, T. Takada, H. Uehara, S. Iwata, and Q. Li, "Research on charge accumulation characteristics by PEA method and Q(t) method," *IEEE Trans. Instrum. Meas.*, vol. 70, pp. 1–9, 2021, doi: 10.1109/TIM.2021.3055288.

[14] K. Kadowaki, M. Maehata, T. Kaji, S. Ito, S. Yudate, and R. Ozaki, "Simultaneous measurement of space charge distribution and leakage current in 6.6 kV CV cable under polarity-reversed voltage," in *Proc. Int. Symp. Electr. Insulating Mater. (ISEIM)*, Sep. 2023, pp. 53–56.

[15] T. G. Aakre, R. Skattenborg, and E. Ildstad, "Limitations regarding use of the ABC-model for interpretation of partial discharge measurements," in *Proc. 26th NORD-IS*, Tampere, Finland, 2019, pp. 10–15, doi: 10.5324/nordis.v0i26.3267.

[16] T. Venge and C. Nyamupangedengu, "Analysis of cavity PD characteristics' sensitivity to changes in the supply voltage frequency," *Energies*, vol. 14, no. 2, p. 478, Jan. 2021, doi: 10.3390/en14020478.

[17] R. M. Christensen, *Mechanics of Composite Materials*. New York, NY, USA: Dover, 2005.

[18] F. Otero, S. Oller, X. Martinez, and O. Salomón, "Numerical homogenization for composite materials analysis. Comparison with other micro mechanical formulations," *Compos. Struct.*, vol. 122, pp. 405–416, Apr. 2015, doi: 10.1016/j.compstruct.2014.11.041.

[19] N. W. Ashcroft and N. D. Mermin, *Solid State Physics*. New York, NY, USA: Thomas Learning, 1976.

RYOTA KITANI received the B.Eng. and M.S. degrees in energy science from Kyoto University, in 2012 and 2015, respectively. Currently, he is with the Osaka Research Institute of Industrial Science and Technology as a Research Scientist. His research interests include electrical degradation, continuum mechanics, computer science, and reliability of electrical product and systems.

SHINYA IWATA (Member, IEEE) received the B.Eng. degree from the Kyoto Institute of Technology, in 2005, and the M.Eng. and Ph.D. degrees from The University of Tokyo, in 2007 and 2011, respectively. Currently, he is with the Osaka Research Institute of Industrial Science and Technology as a Senior Research Scientist. His research interests include electrical degradation, partial discharge, molecular dynamics, quantum chemistry, and reliability of electrical product and systems.

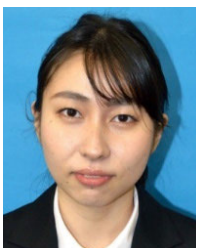

TOMOKA TSUYA received the B.Eng., M.Eng., and Ph.D. degrees from Osaka Prefecture University, in 2017, 2019, and 2022, respectively.

Currently, she is with the Osaka Research Institute of Industrial Science and Technology as a Research Scientist. Her research interests include electrical degradation, partial discharge, preview control, and reliability of electrical product and systems.